JOURNAL OF AIRCRAFT
Vol. 52, No. 4, July–August 2015

Significance of Geometric Nonlinearity in the Design of Thermally Loaded Structures

Joshua D. Deaton* and Ramana V. Grandhi†
Wright State University, Dayton, Ohio 45435

DOI: 10.2514/1.C032872

In reality, all structures exhibit some degree of nonlinearity; however, in many cases, its effects are negligible to the overall structural response and it is common to treat them as such in analysis and design optimization. Due in large part to this practice, severe consequences and structural failures may arise when this nonlinearity cannot be neglected. Currently, this occurs with increasing frequency as designers continue to explore innovative aircraft concepts that push the limits of existing design tools and industry standards. In this research, such a case is investigated where geometrically nonlinear effects result from an elevated temperature environment. The thermoelastic response of characteristic aerospace structures is investigated by comparison of linear and nonlinear analysis results. Results indicate that geometric nonlinearity, which manifests as stress stiffening behavior and deformation-dependent load contributions, plays a significant factor in properly predicting the structural response for structures found in modern military aircraft with embedded engines. In addition, parametric studies present the influence of geometry parameters and boundary fixivity, or how components are attached to adjoining structures, on the nonlinearity in order to identify features that make it critical. Based on these observations, some guidelines regarding when geometric nonlinearity should be included in the structural analysis of thermally loaded structures are provided. These guidelines are useful to the structural analyst or designer faced with the analysis of components in a thermal environment due to engine heat, aerodynamic effects, or other sources.

Nomenclature

A	=	cross-section area
$\boldsymbol{b}$	=	body forces
E	=	elastic modulus
$\boldsymbol{E}$	=	Green–Lagrange strain
$\boldsymbol{F}$	=	deformation gradient
$\boldsymbol{F}_a$	=	applied force vector
$\boldsymbol{F}_b$	=	body force vector
$\boldsymbol{F}_{\text{th}}$	=	thermal load vector
I	=	area moment of inertia
$\mathbf{I}$	=	identity matrix
$\mathbf{K}$	=	stiffness matrix
K_a	=	axial spring stiffness
K_r	=	rotational spring stiffness
k_a	=	axial stiffness ratio
k_r	=	rotational stiffness ratio
L	=	span length
P	=	material point in deformed body
P_o	=	material point in undeformed body
$\boldsymbol{S}$	=	second Piola–Kirchoff stress
T	=	temperature
t	=	thickness
$\boldsymbol{t}^p$	=	prescribed surface traction
$\boldsymbol{U}$	=	displacement vector
$\boldsymbol{u}$	=	displacement field
$\boldsymbol{u}^p$	=	prescribed displacement
$\boldsymbol{X}$	=	undeformed material point position
$\boldsymbol{x}$	=	deformed material point position
α	=	coefficient of thermal expansion
δ	=	curvature measure
$\boldsymbol{\epsilon}$	=	engineering strain
ν	=	Poisson's ratio
$\boldsymbol{\tau}$	=	Cauchy stress
Ω	=	deformed body
Ω_o	=	undeformed body

Received 24 February 2014; accepted for publication 4 March 2014; published online 13 June 2014.

*Graduate Research Assistant, Department of Mechanical and Materials Engineering. Student Member AIAA.

†Distinguished Professor, Department of Mechanical and Materials Engineering. Fellow AIAA.

I. Introduction

IT IS understood that the response of all structural components across any engineering industry includes some amount of nonlinear effect. However, in most cases, the significance of nonlinear effects is small enough, such that the nonlinearity may be neglected for the purposes of engineering analysis and design. As a result, structural design practices and computational tools based on linear physics have become commonplace in the aircraft design process. A troublesome consequence arises when structural nonlinearity cannot be neglected, which in the modern day frequently occurs with innovative aircraft configurations. These configurations promise improved capabilities and performance but also push the limits of existing design tools, historical insight, and industry "rules of thumb." In these cases, the potentially detrimental effects of structural nonlinearity, which are not captured by linear analysis-based design tools, often do not become evident until late stages of detailed design, during experimental or prototype testing, or, in the worst case, during operation of a vehicle. One instance where the impact of nonlinear effects on the structural response is not particularly well understood occurs when structures are exposed to an elevated temperature environment, which is important to current aerospace applications involving embedded engine configurations and sustained high-speed flight [1,2]. In these applications, conventional practices for the design of thermal structures may not be applied and nonlinear effects produce responses that oppose natural intuition for structural design [3].

In this research, we investigate structural nonlinearity for thermally loaded structures and demonstrate its effect on the behavior of thin-plate and shell-like structures, which are important in aircraft construction. We discuss the source and significance of the nonlinearity and identify, based on observations of the results, some guidelines regarding when the geometric nonlinearity is vital to properly predicting the correct thermoelastic response for the class of structures investigated. The remainder of Sec. I introduces the basic types of material and geometric nonlinearity found in aerospace

thermal structures and highlights some conditions where nonlinear effects become critical. Section II includes the mathematical representation of thermoelasticity and a brief overview of how the equations are treated in both linear and nonlinear analyses. A demonstration of nonlinearity results using a characteristic thin structure is provided in Sec. III. Finally, Sec. IV contains concluding remarks.

The analysis of an aircraft structural component subjected to a thermal environment can include both material and geometric nonlinearities. Material nonlinearity occurs in the absence of a linear relationship between stress and strain, such as material yielding, and when material properties become time dependent: for example, in cases of creep or rate-dependent plasticity. In aerospace thermal structures, material nonlinearity also results from the temperature dependence of engineering materials; however, due to the quasi-steady behavior of thermally loaded components, it is easily addressed for the majority of applications [4]. In quasi-steady analysis (also called sequentially coupled or uncoupled thermal-structural analysis), discrete temperature distributions obtained from heat transfer analysis are applied to a structural model to determine its thermoelastic response. For each temperature distribution, a separate structural analysis is performed with the structural properties assigned according to the temperature at each material point. This procedure is appropriate even when linear structural behavior is assumed and does not otherwise require special consideration.

Geometric nonlinearity, on the other hand, relates to nonlinearity in the strain-displacement relationship or changes in the boundary conditions or loading of a structure due to its deformation. These effects are apparent in structures that become either more or less stiff as they deform and in loading for which the magnitude or direction varies with displacement. In reality, all structures exhibit some form of geometric nonlinear behavior, but in many applications, nonlinear contributions to the overall system response are negligible. When this is true, simplifying assumptions related to the magnitude of structural deformation and strains are used to remove nonlinearity from the mathematical representation of the physical problem and computationally efficient linear analysis methods are applied to predict the structural response. These linear representations are standard in the design of aircraft structures where designers desire rapid predictions of the structural response to parametric variations as well as in structural optimization where analytical sensitivity information is readily obtained from linear analysis with little to no computational overhead. To date, linear elastic structures have also been used to form the basis of design sensitivity analysis formulations for thermoelastic structures [5–9]. In fact, challenges related to geometric nonlinearity make sensitivity analysis and design optimization with these responses a formidable task even without thermoelastic contributions.

Historically, geometric nonlinearity in aerospace thermal structures is associated with the stability and postbuckling of plate and shell-like components, both of which are associated with their out-of-plane displacement response, as detailed in the review by Thornton [10]. As a result, in addition to the development of predictions for critical buckling temperatures, researchers have investigated nonlinearity in the out-of-plane response of postbuckled flat plates, plates with initial imperfections or shallow curvature, and cylindrical and conic shells of revolution. To create nonlinear out-of-plane deformation in these structures, thermal expansion must be restrained such that it generates sufficient bending moments. Conveniently, a fundamental design rule, which is to accommodate thermal expansion to prevent damaging thermal stresses, has also been applied to the design of thermal structures for over 50 years, with notable applications including those in atmospheric reentry and high-speed flight vehicles [4,11]. Apart from a few exceptions [12,13], this led to the consideration of cases where the thin-plate and shell structures are free to expand in plane and free to undergo rotation about their edges, which is consistent with design applications where thermal expansion can be easily accommodated. As such, the necessary conditions of restrained expansion for geometric nonlinearity occur only in cases where significant spatial temperature gradients across a plate or shell provide a sufficient mismatch in thermal expansion, which is often not possible in typical operating environments. However, the conditions for nonlinearity can be more readily generated in situations where thermal expansion is restrained in plane by boundary fixity, which by the nature of historical applications and design practices have not been as widely addressed in the literature. This circumstance is found in modern thermal structures applications related to embedded engine aircraft. Here, design scenarios are found where thermal expansion cannot be easily accommodated, and thus may be prone to nonlinear responses due to aircraft configuration-level requirements like low observability.

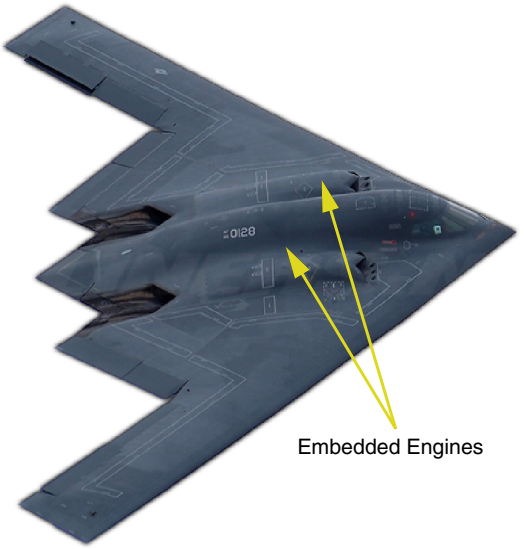

Fig. 1 B-2 Spirit stealth bomber with embedded engine configuration.

Burying aircraft engines inside the airframe, as is done in the B-2 Spirit stealth bomber, shown in Fig. 1, affords tremendous tactical capabilities. This embedded engine configuration allows for a smooth outer mold line, reduced exhaust noise, and cooler exhaust gases, which all reduce the vehicle's observability by decreasing radar, acoustic, and infrared detectability [14]. In addition, by using a ducted exhaust system, direct line of sight into hot engine components is prevented, denying the enemy a vulnerable infrared target. However, these tactical advantages come at the cost of added structural design complexity. Structural components, known as exhaust-washed structures, which make up the flowpath for exhaust as it exits the aircraft, are exposed to high temperatures and are rigidly fixed to supporting structure to maintain smooth continuity for both observability and flow considerations. Figure 2 shows a schematic of an exhaust-washed structure and surrounding substructures from a conceptual embedded engine aircraft. As a result of the elevated temperature and boundary fixity, the static response of the panel and shell-like exhaust structures is characterized by out-of-plane deformation and excessive stresses at the connections to supporting substructures. In fact, this response can contain significant geometric nonlinearity and has important implications for the design of these components. This has provided the impetus for the conceptual and numerical investigations in this paper, from which we glean conclusions regarding the nature of this type of nonlinearity and guidelines concerning the geometric and parametric factors that make it significant.

II. Thermoelastic Formulation

The behavior of a structural component subjected to combined mechanical and thermal loading is governed by the equations of thermoelasticity along with appropriate initial and boundary conditions. In the formulation of these equations, the linearity of the resulting boundary value problem is determined by the choice of stress and strain measures. The development of these equations for both nonlinear and linear analyses in the absence of thermal effects can be found in several continuum mechanics texts [15]. Thus, we

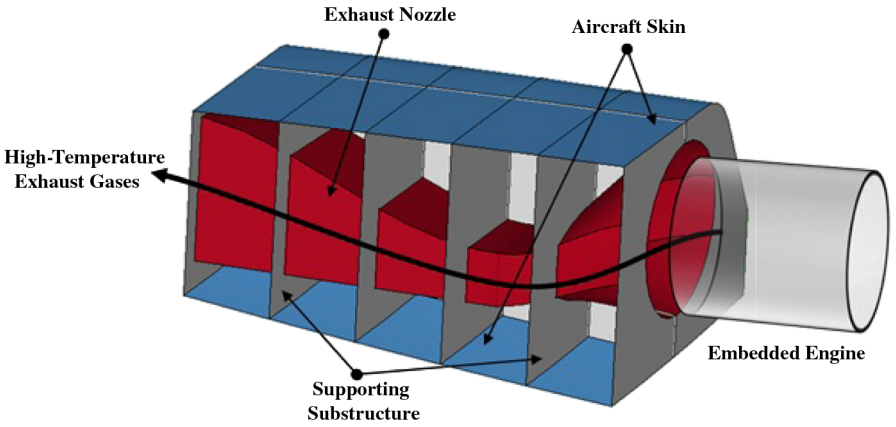

Fig. 2 Conceptual engine exhaust-washed structure configuration located aft of embedded engines on a low observable aircraft.

highlight only the resulting sets of equations with thermal loading, which requires including the appropriate thermal strain terms in the constitutive equations. In addition, we comment on the typical method of solution by the finite element method for each case. In the proceeding discussion, we assume that structural analysis is performed based on a prescribed temperature distribution that does not depend on the deformation state of the structure. This is consistent with the typical uncoupled or quasi-steady formulations discussed earlier. As a result, all material constants are assumed to be taken at the prescribed temperature of a given material point.

A. Geometric Nonlinear Formulation

In nonlinear analysis, an important distinction is drawn between the undeformed configuration Ω_o of a body and its deformed configuration Ω after loading. These states are shown in Fig. 3.

Using a Lagrangian description, the location of a material point P_o in Ω_o is given by the position vector $\boldsymbol{X}$. After experiencing a displacement field $\boldsymbol{u}(\boldsymbol{X})$, the location of the point P in Ω is given by $\boldsymbol{x}(\boldsymbol{X})$. The deformation gradient $\boldsymbol{F}$ relates the undeformed and deformed configurations with the derivative of each component of the deformed position $\boldsymbol{x}$ with respect to each component of the reference position $\boldsymbol{X}$. Noting that

$$\boldsymbol{x} = \boldsymbol{X} + \boldsymbol{u} \tag{1}$$

the deformation gradient is

$$\boldsymbol{F}(\boldsymbol{X}) = \mathbf{I} + \frac{\partial \boldsymbol{u}}{\partial \boldsymbol{X}} \tag{2}$$

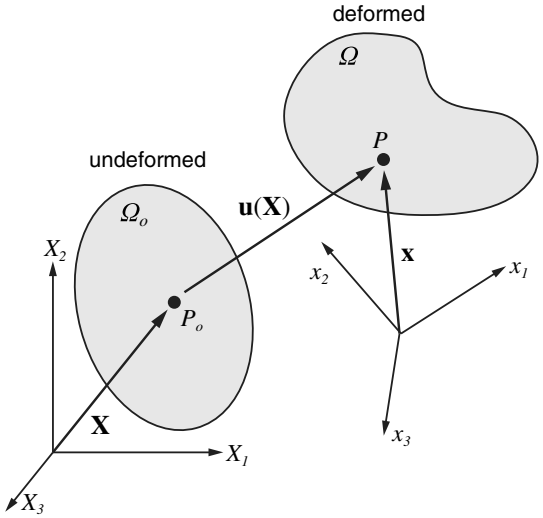

Fig. 3 Undeformed reference and deformed configurations of a continuum body.

The Green–Lagrange strain $\boldsymbol{E}$ is given in terms of the deformation gradient and displacement as

$$\boldsymbol{E} = \frac{1}{2}(\boldsymbol{F}^T\boldsymbol{F} - \mathbf{I}) = \frac{1}{2}\left(\frac{\partial \boldsymbol{u}}{\partial \boldsymbol{X}} + \frac{\partial \boldsymbol{u}}{\partial \boldsymbol{X}}^T + \frac{\partial \boldsymbol{u}}{\partial \boldsymbol{X}}^T \frac{\partial \boldsymbol{u}}{\partial \boldsymbol{X}}\right) \tag{3}$$

where $\mathbf{I}$ is the identity matrix. The Green–Lagrange strain is used as the kinematic (strain-displacement) relationship for geometric nonlinear analysis. The equilibrium equations are given by

$$\mathrm{div}(\boldsymbol{F}(\boldsymbol{X})\boldsymbol{S}(\boldsymbol{X})) + \boldsymbol{b}(\boldsymbol{X}) = 0 \tag{4}$$

where $\boldsymbol{b}$ is the body force vector defined per unit undeformed volume, and $\boldsymbol{S}(\boldsymbol{X})$ is the second Piola–Kirchoff stress. We note that this stress measure is energetically conjugate to the Green–Lagrange strain and, unlike the usual Cauchy stress tensor $\boldsymbol{\tau}$, is defined on the undeformed configuration of the body. In practice, $\boldsymbol{S}$ is used in the solution of the thermoelasticity equations, but the Cauchy stress is determined from

$$\boldsymbol{\tau} = \boldsymbol{F}\boldsymbol{S}\boldsymbol{F}^T \tag{5}$$

and used for the engineering stress response. This is done because most engineering design criteria are based on the Cauchy stress, and the components of the second Piola–Kirchoff stress lack physical meaning. For an isotropic material that remains elastic, the constitutive equations (stress–strain relationship) in terms of the Green–Lagrange strain and second Piola–Kirchoff stress are given by

$$\boldsymbol{E} = \frac{1}{E}[(1+\nu)\boldsymbol{S} - \nu\mathbf{I}tr(\boldsymbol{S})] + \alpha T(\boldsymbol{X})\mathbf{I} \tag{6}$$

where ν is the Poisson's ratio, E is the elastic modulus, α is the coefficient of thermal expansion, and $T(\boldsymbol{X})$ is a temperature change defined on the undeformed configuration. Finally, the essential and natural boundary conditions are given using prescribed displacements $\boldsymbol{u}^p$ and surface tractions $\boldsymbol{t}^p$ on the undeformed configuration as

$$\boldsymbol{u}(\boldsymbol{X}) = \boldsymbol{u}^p(\boldsymbol{X}) \tag{7}$$

$$\boldsymbol{F}(\boldsymbol{X})\boldsymbol{S}(\boldsymbol{X})\boldsymbol{n}(\boldsymbol{X}) = \boldsymbol{t}^p(\boldsymbol{X}) \tag{8}$$

where $\boldsymbol{n}$ is a unit normal vector for the surface on which $\boldsymbol{t}^p$ is defined.

B. Linear Formulation

The thermoelastic equations for linear analysis are formulated under the assumption that displacements are sufficiently small such that no distinction is necessary between the undeformed and deformed configurations and the deformation gradient in the nonlinear formulation becomes the identity matrix. In addition, it is assumed the displacement gradients are sufficiently small such that

their products may be neglected. As a result, the Green–Lagrange strain, given by Eq. (3), is reduced to the engineering strain $\boldsymbol{\epsilon}$ by neglecting second-order gradients

$$\boldsymbol{\epsilon} = \frac{1}{2}\left(\frac{\partial \boldsymbol{u}}{\partial \boldsymbol{X}} + \frac{\partial \boldsymbol{u}^T}{\partial \boldsymbol{X}}\right) \tag{9}$$

With no delineation between the body's configuration before and after displacement, the equilibrium equations can be given directly in terms of the Cauchy stress $\boldsymbol{\tau}$ and body forces $\boldsymbol{b}$ as

$$\mathrm{div}(\boldsymbol{\tau}(\boldsymbol{X})) + \boldsymbol{b}(\boldsymbol{X}) = 0 \tag{10}$$

The constitutive equation in Eq. (6) is used again for an elastic material, but it is now written in terms of the engineering strain and Cauchy stress by

$$\boldsymbol{\epsilon} = \frac{1}{E}[(1+\nu)\sigma - \nu \mathbf{I}\, tr(\tau)] + \alpha T(\boldsymbol{X})\mathbf{I} \tag{11}$$

Finally, constraints are specified to complete the boundary value problem by

$$\boldsymbol{u}(\boldsymbol{X}) = \boldsymbol{u}^p(\boldsymbol{X}) \tag{12}$$

$$\tau(\boldsymbol{X})\boldsymbol{n}(\boldsymbol{X}) = \boldsymbol{t}^p(\boldsymbol{X}) \tag{13}$$

C. Solution by Finite Element Methods

In structural analysis, it is common to recast the elastic equations into a discrete form using variational or Galerkin methods to be solved using finite elements. After doing so, discretizing the body, and summing element contributions, a global set of equations for nonlinear structural finite element analysis may be given by

$$\mathbf{K}(\boldsymbol{U})\boldsymbol{U} = \boldsymbol{F}_a + \boldsymbol{F}_b(\boldsymbol{U}) + \boldsymbol{F}_{\mathrm{th}}(\boldsymbol{U}) \tag{14}$$

where $\mathbf{K}$ is the stiffness matrix, $\boldsymbol{F}_a$ is the vector of applied loads, $\boldsymbol{F}_b$ is the body force vector, $\boldsymbol{F}_{\mathrm{th}}$ is the thermal load vector, and $\boldsymbol{U}$ is the nodal displacement vector. We observe that Eq. (14) is nonlinear in terms of the unknown displacements $\boldsymbol{U}$; and the stiffness matrix, body force vector, and thermal load vector are dependent upon the deformation, as formulated in Sec. II.A. In practice, incremental iterative techniques based on the Newton–Raphson method are used to solve the finite element equations. To account for the dependence of stiffness and load terms on the displacement, the matrices are periodically reformulated throughout the iterative process.

On the other hand, the global equations for a finite element problem formulated under the assumptions in Sec. II.B for linearized physics are given by

$$\mathbf{K}\boldsymbol{U} = \boldsymbol{F}_a + \boldsymbol{F}_b + \boldsymbol{F}_{\mathrm{th}} \tag{15}$$

We note the system is linear in terms of the displacement vector $\boldsymbol{U}$, which is determined using standard solution methods for linear systems.

In the investigation that follows, the commercial finite element software MD Nastran is used using the appropriate solution procedures for both linear and nonlinear representations.

III. Curved Strip Nonlinear Analysis

A parameterized curved strip model is investigated to demonstrate the significance of geometric nonlinearity induced by thermal loads. This simple two-dimensional (2-D) model directly represents a semi-infinite cylindrical shell but also serves as a suitable idealization of the basic components of more complex thin-shell thermal structures. A schematic of the model is shown in Fig. 4b, which represents the 2-D exhaust-washed structure section shown in Fig. 4a. Here, L denotes the span covered by the strip, δ is a measure of curvature (which is assumed as circular), and t is the thickness of the strip. A rectangular cross section with unit width into the page is also assumed. Since boundary conditions are critical in cases of thermal expansion, linear elastic boundaries are used. By varying the values of K_a (axial) and K_r (rotational) stiffness, all cases from fully clamped and simply supported to free expansion can be modeled. In addition, translation of edge nodes in the vertical direction is prevented. Finally, loading consists of a spatially uniform temperature increase T.

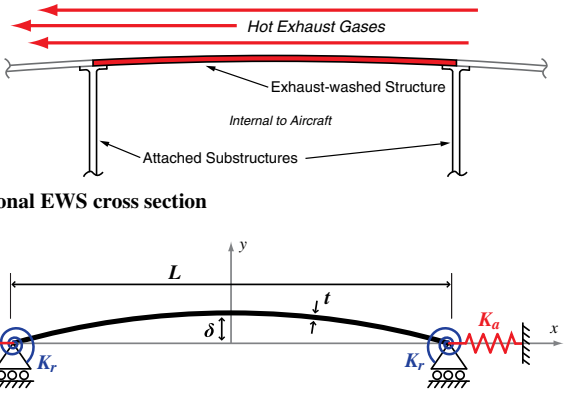

Fig. 4 Representations of a) notional cross section of thin exhaust-washed structure (EWS) attached to supporting substructure and subjected to hot exhaust gases, and b) the corresponding curve strip model (note that curvature is of circular profile).

In the study of thermal structures, often the magnitude of temperature is misleading with respect to the severity of its structural consequences because it does not reflect the material properties. A more suitable indicator of the severity of a given temperature level for a material is the product of its elastic modulus E, the coefficient of thermal expansion (CTE) α, and the elevated temperature T. Examples for various engineering materials at common operational temperatures are given in Table 1. We note that, with respect to the overall effect of temperature loading, a Ceramic Matrix Composite (CMC) component with low CTE may experience nearly the same thermoelastic effects as a titanium alloy due to increased operational temperature in cases with sufficient boundary fixivity or spatial temperature gradients. In the following investigations, structural properties are taken as Ti 6242 from Table 1, but in an attempt to retain generality, we note here that results were observed to scale rather proportionally with $E\alpha T$ in additional tests with various materials and temperature levels.

The curved strip is modeled in MD Nastran using 250 two-node beam elements, which is a sufficient discretization based on mesh convergence. The model inputs are parameterized using a thickness-to-span-length ratio t/L and a curvature-to-span-length ratio δ/L. In practical applications, the thickness-to-span-length ratio t/L ranges from 0.005 to 0.05 and the curvature-to-span-length ratio δ/L ranges from 0.0 (perfectly flat) to 0.5 (half-circle). Finally, in the discussions that follow, comments regarding the accuracy of linear analysis results assume that the nonlinear response predicts the true structural response. In other engineering disciplines using physics-based simulations, nonlinear models may not always be more accurate with respect to experimental results and significant uncertainty exists in the selection of the appropriate mathematical model to correctly represent the physics [19,20].

Table 1 Approximate properties at high operating temperatures

Material	T, °F	E, 10^6 psi	α, 10^{-6}/°F	$E\alpha T$ ($\times 10^3$)
Ti 6242 [16]	900	12.5	5.5	61.68
Inconel 718 [16]	1300	24.0	8.5	265.2
Gr-BMI (0/90) [17]	400	8.0	12.0	38.40
CMC [18]	1700	14.5	2.5	61.62

A. Deformation

The deformation response of the strip model with varying curvature, as predicted by both linear and nonlinear analyses, is given in Fig. 5. In the plots, three thermal conditions are represented by three $E\alpha T$ values. Boundary conditions are specified using elastic elements with $K_a = K_r = \infty$ (Figs. 5a and 5c), which represents a clamped condition, and $K_a = \infty$, $K_r = 0$ (Figs. 5b and 5d), which represents a condition with free rotation over the edge and no translation of edge nodes. The curvature-to-length-span ratios δ/L of 0.01 (Figs. 5a and 5b) and 0.05 (Figs. 5c and 5d) are indicated in the figure. The thickness-to-span-length ratio is taken as $t/L = 0.013$. The black curve denotes the undeformed configuration of the strip absent thermal loads, and the dashed and solid curves represent deformed shapes from linear and nonlinear analyses, respectively.

From Fig. 5, it is evident that the effect of geometric nonlinearity in the deformation response, which is observed as the difference between the linear and nonlinear response curves, increases with $E\alpha T$ regardless of boundary type and amount of curvature. However, when comparing Figs. 5a and 5b to Figs. 5c and 5d, we see that this effect is much less pronounced in the strip of greater curvature. In addition, linear analysis overpredicts the out-of-plane deformation response as the severity of thermal loading increases (note that this observation is not general to all thicknesses, as will be shown in forthcoming results). We also note that, when using linear analysis, the magnitude of deformation increases monotonically with $E\alpha T$, assuming temperature-independent properties. This is not observed in the nonlinear response, where the effects of stress stiffening and follower forces preclude this nonphysical behavior. This is especially evident in the strips of low curvature in Figs. 5a and 5b, with free rotation boundaries exhibiting the greatest discrepancy between linear and nonlinear analyses.

B. Effect of Geometric Parameters

To understand the effect of geometric or dimensional parameters on the significance of nonlinearity, we now perform a parametric study by varying the thickness of the strip for different values of curvature. Figure 6a shows the vertical displacement measured at the center of the strip (normalized by the span length L), and Fig. 6c shows the maximum stress as a function of thickness t/L for four values of curvature δ/L and clamped boundaries ($K_a = \infty$, $K_r = \infty$). Figures 6b and 6d show analogous results for free rotation boundaries ($K_a = \infty$, $K_r = 0$). Here, $E\alpha T = 60 \times 10^3$. This level of thermal loading was selected based on deformation plots, which indicated that the difference between linear and nonlinear analyses is most severe at the greatest values of $E\alpha T$. As mentioned earlier, this value corresponds to typical conditions for a high-temperature titanium alloy, but the observations here are readily extendable to other material systems.

In all of the plots shown in Fig. 6, we see that increasing the curvature (denoted by different curves) reduces the difference between linear and nonlinear analysis predictions for a large variety of strip configurations. In fact, for curvatures of $\delta/L = 0.150$ (and greater), no appreciable difference in displacements or stresses is evident. This is due to the fact that a curved strip is initially nearer to the thermally loaded equilibrium configuration. As a result, the effect of deformation dependent forces, which are neglected in linear analysis where the loads are applied to only the undeformed structure, is reduced. When using a nonlinear analysis procedure, the direction of the loads that result from thermal expansion remains consistent with the deformed configuration via periodic updating.

More interesting than simply the difference between the analyses are the trends that result for parametric variations in thickness t/L. In each plot, we see that, for strips of larger curvature (curves), the

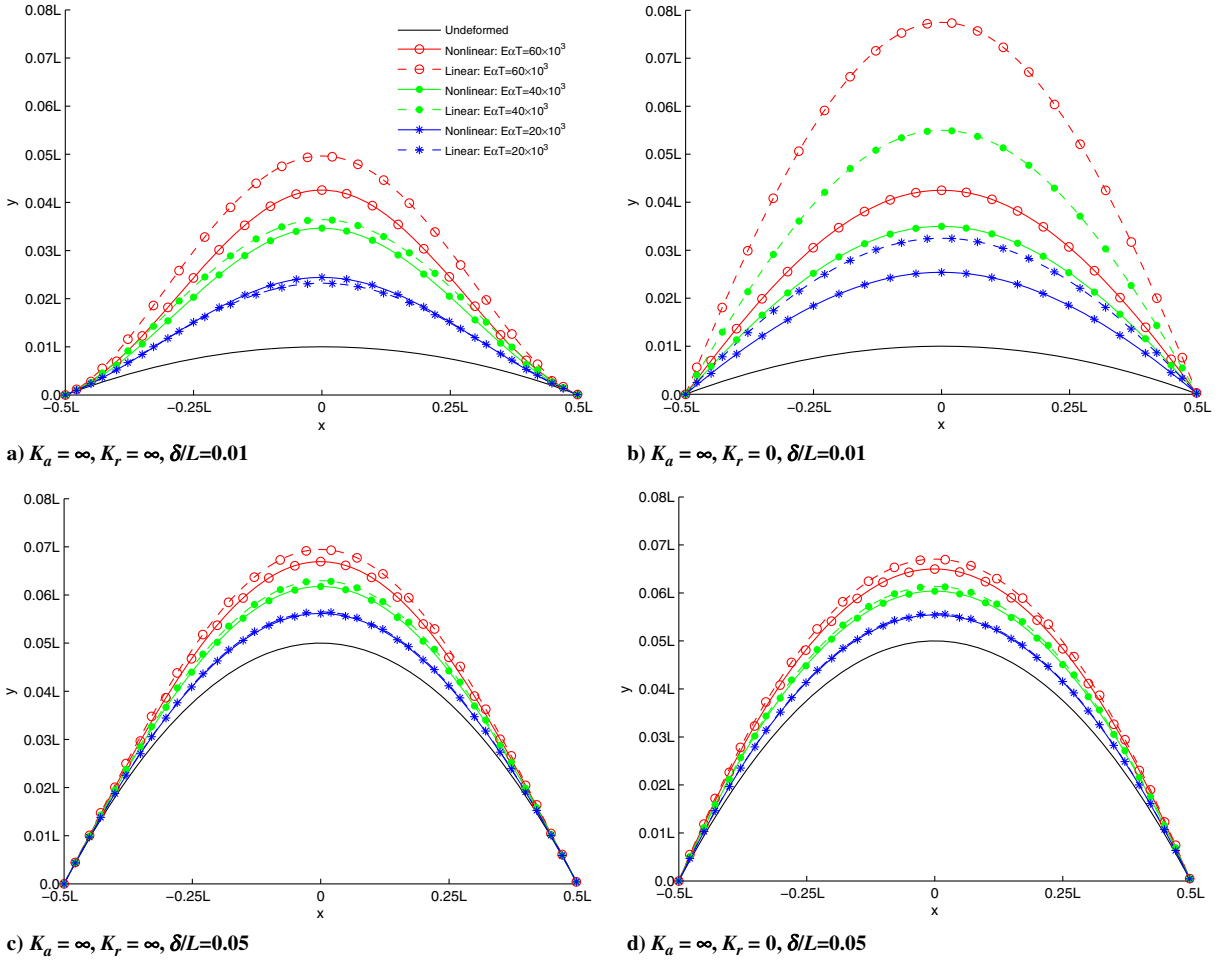

a) $K_a = \infty$, $K_r = \infty$, δ/L=0.01

b) $K_a = \infty$, $K_r = 0$, δ/L=0.01

c) $K_a = \infty$, $K_r = \infty$, δ/L=0.05

d) $K_a = \infty$, $K_r = 0$, δ/L=0.05

Fig. 5 Deformation of curved strip for various boundary conditions and curvature-to-length-span ratios.

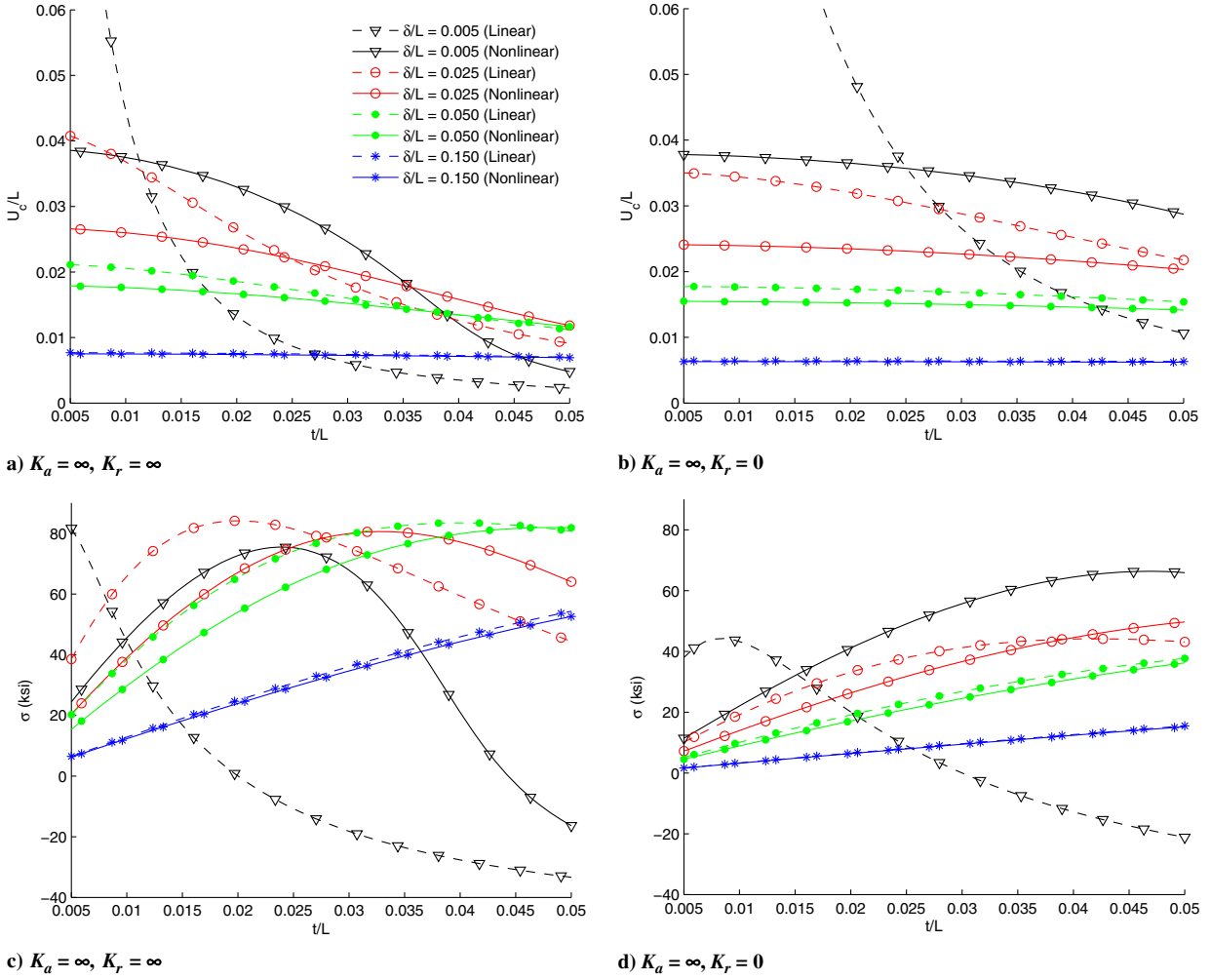

a) $K_a = \infty$, $K_r = \infty$ b) $K_a = \infty$, $K_r = 0$

c) $K_a = \infty$, $K_r = \infty$ d) $K_a = \infty$, $K_r = 0$

Fig. 6 Representations of a, b) center displacement and c, d) maximum stress as functions of thickness ratio for multiple curvature ratios ($E\alpha T = 60 \times 10^3$).

general trend for increasing thickness is similar for both linear and nonlinear analyses. This observation is important when considering the effect of nonlinear analysis in the design and optimization of thermal structures. It implies that, for structures for which the configuration contains sufficient curvature, linear analysis may contain error but yields the proper trends in response variability. This aspect is critical when performing trade studies and design space exploration early in a design process. On the other hand, for a curvature ratio $\delta/L = 0.005$ (black curve), which corresponds to a strip with little curvature, linear and nonlinear analyses respond completely different to parametric variations in thickness. This indicates that the linear analysis fails to correctly capture the fundamental physics governing the displacement and stress responses, which we may now assume are considerably nonlinear.

Further investigation into the plots of Fig. 6 yields a great deal of insight regarding the parametric effect on geometric nonlinearity. For example, for greater curvature ratios, increasing the thickness reduces the discrepancy between linear and nonlinear analyses; however, for nearly flat geometry, the differences persist over an order of magnitude of thickness variation (t/L from 0.005 to 0.05). In addition, instances are observed where the need for nonlinear analysis is not obvious based on conventional structural design rules of thumb, which are largely based on mechanical responses without thermoelastic considerations. For example, the occurrence of displacement in a beam or plate structure that approaches or exceeds its thickness is a common indication of the need for nonlinear analysis. In this case, the effects of stress stiffening, or the coupling between transverse displacement and membrane stiffness that is neglected in the kinematic relations of linear analysis, become significant. In all plots in Fig. 6 with greater curvatures, we observe cases where displacement is multiple times greater than the strip thickness, but linear analysis predicts the response with excellent accuracy compared to nonlinear analysis. However, for strips of low curvature and high thickness (in excess of $t/L = 0.025$ in Fig. 6a), we observe a case where geometric nonlinearity is significant, but the displacement predicted by linear analysis is less than 25% of the thickness. This observation indicates that traditional insights for structural analysis may not accurately reflect the need for nonlinearity in thermoelasticity.

C. Effect of Boundaries

To this point, we have only investigated models with simple boundary conditions with fixed degrees of freedom, which represented extreme cases of rigid fixivity for thermal expansion. In reality, the true boundary conditions of thermally restrained structures depend on the stiffness of surrounding components as well as the type of joints. To understand the implications of boundaries with finite stiffness, we now use the spring conditions in Fig. 4b. A parametric study similar to the preceding investigations, with varying thickness ratios and multiple curvatures, is performed; however, rather than rigid fixivity, finite values of rotational and axial stiffness are systematically prescribed. To provide relational context to the magnitude of stiffness boundaries, the spring stiffness values K_a and K_r are parameterized as

$$K_a = k_a \frac{AE}{L} \tag{16}$$

$$K_r = k_r \frac{EI}{L^2} \tag{17}$$

Here, we note two quantities provide estimations for the stiffness of the strip itself. In Eq. (16), AE/L is analogous to the stiffness of a flat axial bar, where A is the cross section area, E is the elastic modulus, and L is the length. Similarly in Eq. (17), EI/L^2 is analogous to the bending stiffness of a flat cantilever beam when I equals the moment of inertia. If K_a and K_r are taken as the stiffness of adjoining structures, the parameters k_a and k_r represent an approximation for the ratio between the stiffness of the adjoining structure (or boundary stiffness) and the stiffness of the strip itself in the axial and rotational directions, respectively. It is noted that these quantities hold truly physical meaning only for flat strips; however, they still provide a convenient approximation of the magnitude of boundary stiffness when curvature is not excessive. For clarity, a unit value of k_a or k_r indicates the boundary has approximately equal stiffness to the strip, whereas a large or small (fractional) value asserts that the boundary has a much greater or lower stiffness than the strip in that dimension, respectively.

Figure 7 shows the maximum stress in the strip as a function of thickness for multiple values of finite rotational stiffness. In the axial direction, zero displacement at the boundaries is prescribed ($K_a = \infty$). We note that the current value of thickness is used in the determination of boundary stiffness in Eqs. (16) and (17). Additional studies considering fixed thickness for the boundary stiffness calculation resulted in similar results for trends in stress as a function of thickness. Figure 7a shows results for $\delta/L = 0.005$ (nearly flat), and Fig. 7b shows results for $\delta/L = 0.050$ (modest curvature). Comparing the trends with increasing thickness in each case, we again observe that, with greater curvature, linear analysis is better able to capture the trend in parametric stress response. For strips with little curvature, just as in Fig. 6, the structural response is governed by nonlinear effects. This observation holds for all values of k_r in Fig. 7a. On the other hand, Fig. 7b indicates that the stress response for lower values of rotational stiffness k_r is more accurately predicted by linear analysis when modest curvature in the geometry is present. This implies that, to some extent, rotational stiffness at boundaries activates some nonlinear effects, as exhibited by significant differences around $k_r = 500$ and greater in this case. This is likely due to its strong influence on the out-of-plane displacement of the strip.

Figure 8 shows the maximum stress results as a function of thickness for multiple values of k_a. Here, zero rotational displacement is prescribed ($K_r = \infty$) and results are again given for two values of curvature. Similar to the previous case, we observe that the response of the strip with greater curvature in Fig. 8b is better captured by linear analysis than that with little curvature in Fig. 8a. On first inspection, it may appear that, in Fig. 8a, linear analysis captures a trend of decreasing stress with increasing thickness for strips of thickness greater than approximately $t/L = 0.025$, but noting the state of stress (indicated by its sign), we conclude otherwise. Here, linear analysis predicts a state of purely compressive stress at much lower thickness values, which again alludes to the dominance of nonlinear effects in the out-of-plane (bending) deformation behavior. Similar to the cases of rotational stiffness, from Fig. 8b, increasing axial stiffness appears to increase the difference in analysis predictions, with differences becoming significant above approximately $k_a = 3$. This is again attributed to the contribution of boundary stiffness to the out-of-plane deformation that results. Finally, it may be concluded that, while both axial and rotational boundary stiffnesses do contribute to the nonlinearity, the effect appears to be much less pronounced than changes in the strip curvature. In fact, the inability of linear analysis to capture the proper trends in displacement and stress as observed in Figs. 7a and 8a results from a lack of curvature. In the nearly flat geometries, capturing the effects of deformation on the orientation of thermal stress contributions using iterative updating as done in nonlinear analysis is critical.

D. Nonintuitive Design Responses

To this point, investigations have been performed to identify characteristics that play a role in the significance of geometric nonlinear in the thermoelastic response. With this understanding, we now discuss the behavior of the response itself rather than comparisons between the results of different analysis types. Here, we continue to regard the nonlinear results as the true structural behavior and explore the nonintuitive effects of parametric variation and the implications of nonlinearity in design responses.

Referring back to Figs. 7 and 8, which give the maximum stress in the strip as a function of the thickness, we observe interesting parametric stress behavior across a wide variety of geometries and boundary conditions. Remarkably, in each plot, we observe increases in the maximum stress as the thickness is increased, especially beginning at low values of t/L. This behavior is unique to structures with so called design-dependent loading, which includes temperature loads, and is counterintuitive when compared to mechanically loaded structures. It was also specifically noted to pose significant challenges in the preliminary structural sizing study of a hypersonic vehicle [21]. One of the most common techniques for reducing stresses in mechanically loaded structures is to increase their stiffness by increasing size parameter of the component. In the thin structures

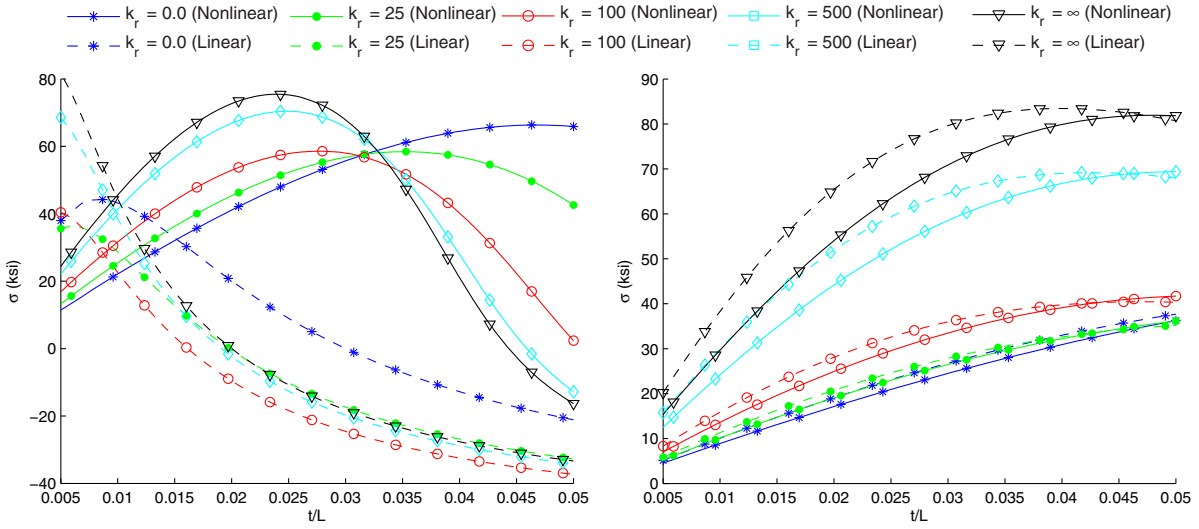

a) $K_a = \infty$, K_r = variable, $\delta/L = 0.005$ b) $K_a = \infty$, K_r = variable, $\delta/L = 0.050$

Fig. 7 Maximum stress in the strip as a function of thickness with finite values of rotational boundary stiffness and curvatures of a) $\delta/L = 0.005$ and b) $\delta/L = 0.050$ ($E\alpha T = 60 \times 10^3$).

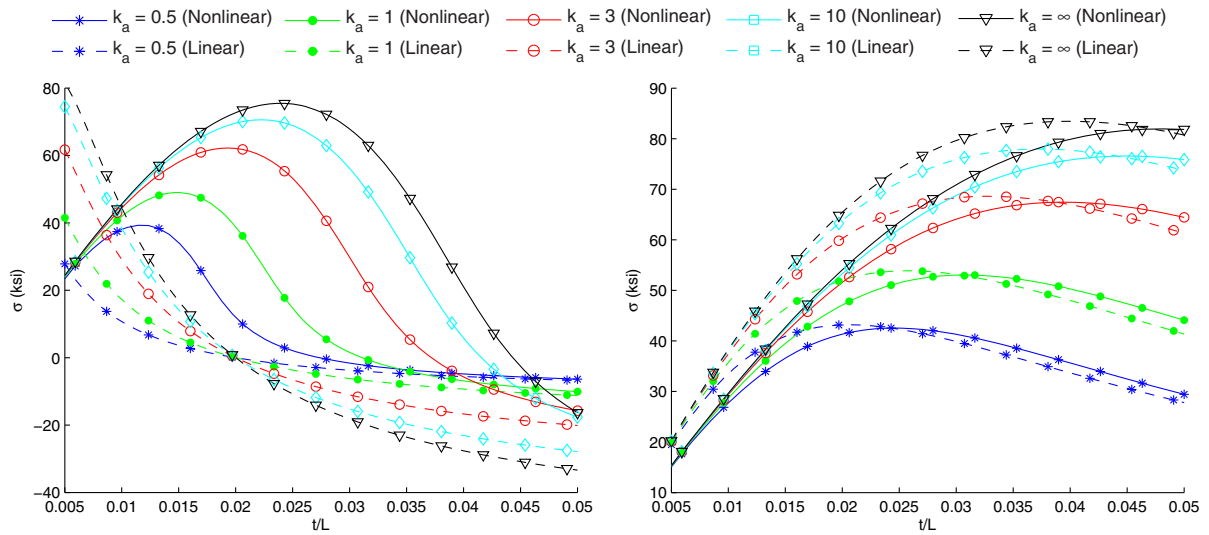

a) K_a = variable, $K_r = \infty$, $\delta/L = 0.005$ b) K_a = variable, $K_r = \infty$, $\delta/L = 0.050$

Fig. 8 Maximum stress in the strip as a function of thickness with finite values of axial boundary stiffness and curvatures of a) $\delta/L = 0.005$ and b) $\delta/L = 0.050$ ($E\alpha T = 60 \times 10^3$).

considered here, this corresponds to increasing the thickness. Contrary to mechanical loading, the design dependency of temperature loading results in additional thermal loading from the added material that also undergoes thermal expansion. Thus, in some circumstances represented in Figs. 7 and 8, the proper prescription for reducing thermal stresses is actually to reduce the thickness. In practice, this may not always be possible when considering other design requirements related to vibration and dynamic stability. In some cases shown in the same figures, we do see that, for higher values of t/L, increasing the thickness can lead to stress reduction, particularly in cases with high (or infinite) stiffness in the rotational direction at boundaries. However, we note that, if considering an initially thin structure, significant increases in thickness (exceeding three to five times the original thickness) are required to realize a reduction in stress. This translates to significant increases in structural weight. In addition, when comparing Fig. 7a to Fig. 7b and Fig. 8a to Fig. 8b, we observe that the effectiveness of this treatment diminishes with added curvature in the geometry.

Most important to the focus of this paper is the observation that, in Figs. 7a and 8a, linear analysis completely fails to capture this trend in structures with low values of curvature δ/L due to the inability of linear analysis to capture the deformation dependency of the thermal stress to loading. More than anything, this reinforces the practical significance of nonlinearity in this thermoelastic design domain. Take for example the design of a structure with nearly clamped boundaries and low curvature of $\delta/L = 0.005$, which can be found in Fig. 8a. Linear analysis of an initially thin strip will yield stress results that significantly overpredict the true value. Moreover, a parametric study with linear analysis implies that excessive stress can be reduced by increasing the thickness. This would result in a critically failed design, as observed from the nonlinear predictions, which show that by even doubling the thickness of initially low thickness components may actually result in greater than a twofold increase in stresses.

IV. Conclusions

In most cases, the effects of geometric nonlinearity may be neglected in the design of aircraft structures. One instance where this common practice produces detrimental consequences is in the design of thin thermal structures. Depending on boundary fixivity, the effects of geometric nonlinearity govern the out-of-plane deformation response of the characteristic geometries, which are present on modern military aircraft featuring buried engines. In this research, several fundamental studies were performed to assess the factors that contribute to the nonlinearity. Based on the results, the following general conclusions may be drawn and may be used as approximate design guidelines:

1) Increasing temperatures (or increasing $E\alpha T$) increases the effect of geometric nonlinearity.

2) The effect of varying thickness on geometric nonlinearity appears to be small compared to other factors.

3) Increasing the curvature reduces the effect of geometric nonlinearity.

4) Increasing both rotational and axial stiffnesses of boundaries increases the significance of geometric nonlinearity.

Regarding the previous effects on nonlinearity, the curvature (or lack of) is the most important factor. It is suggested that geometric nonlinear analysis be used for any thin thermally loaded component for which the out-of-plane curvature is less than 5% of the total span covered if boundary conditions are sufficient to generate an out-of-plane response. Failure to do so will likely lead to structural response predictions that are in no way representative of the true nonlinear physics in this domain.

These geometric nonlinear effects are due in large part to the configuration dependence of the thermal loading, with additional contributions from stress stiffening behavior. The significance of geometric nonlinearity in predicting the response of these types of thermal structures leads to challenges in the application of structural optimization to improve the designs. As a result, additional research of advanced techniques for thermoelastic optimization is critical to the design of future aircraft with low observability considerations and for hypersonic flight thermal protection applications. Due to the similarity of the test structure used here to plate and shell types of structures, it is reasonable to assume that they will behave in much the same way. Thus, care should be taken to investigate geometric nonlinearity in the design of any structure that may undergo out-of-plane deformation due to an elevated temperature environment. Without proper understanding of the effects of variability in this design domain owing to geometric nonlinearity, reduced performance and reliability are likely to result when using conventional design paradigms.

Acknowledgments

The authors would like to acknowledge the support provided by the U.S. Air Force Research Laboratory through contract FA8650-09-2-3938, the Collaborative Center for Multidisciplinary Sciences. The views and conclusions contained herein are those of the authors and should not be interpreted as representing official policies or endorsements, either expressed or implied, of the U.S. Air Force Research Laboratory or the U.S. Government.

References

[1] Haney, M. A., and Grandhi, R. V., "Consequences of Material Addition for a Beam Strip in a Thermal Environment," *AIAA Journal*, Vol. 47, No. 4, 2009, pp. 1026–1034. doi:10.2514/1.41205

[2] McNamara, J. J., and Friedmann, P. P., "Aeroelastic and Aerothermoelastic Analysis in Hypersonic Flow: Past, Present, and Future," *AIAA Journal*, Vol. 49, No. 6, 2011, pp. 1089–1122. doi:10.2514/1.J050882

[3] Deaton, J. D., and Grandhi, R. V., "Stiffening of Restrained Thermal Structures via Topology Optimization," *Structural and Multidisciplinary Optimization*, Vol. 48, No. 4, 2013, pp. 731–745. doi:10.1007/s00158-013-0934-5

[4] Thornton, E. A., *Thermal Structures for Aerospace Applications*, AIAA Education Series, AIAA, Reston, VA, 1996, pp. 141–182.

[5] Bhatia, M., and Livne, E., "Design-Oriented Thermostructural Analysis with External and Internal Radiation, Part 1: Steady State," *AIAA Journal*, Vol. 46, No. 3, 2008, pp. 578–590. doi:10.2514/1.26236

[6] Bhatia, M., and Livne, E., "Design-Oriented Thermostructural Analysis with External and Internal Radiation, Part 2: Transient Response," *AIAA Journal*, Vol. 47, No. 5, 2009, pp. 1228–1240. doi:10.2514/1.40265

[7] Tortorelli, D. A., Subramani, G., and Lu, S. C. Y., "Sensitivity Analysis for Coupled Thermelastic Systems," *International Journal of Solids and Structures*, Vol. 27, No. 12, 1991, pp. 1477–1497. doi:10.1016/0020-7683(91)90073-O

[8] Tortorelli, D. A., Haber, R. B., and Lu, S. C.-Y., "Adjoint Sensitivity Analysis for Nonlinear Dynamic Thermoelastic Systems," *AIAA Journal*, Vol. 29, No. 2, 1991, pp. 253–263. doi:10.2514/3.10572

[9] Meric, R. A., "Material and Load Optimization of Thermoelastic Solids. Part I: Sensitivity Analysis," *Journal of Thermal Stresses*, Vol. 9, No. 4, 1986, pp. 359–372. doi:10.1080/01495738608961912

[10] Thornton, E. A., "Thermal Buckling of Plates and Shells," *Applied Mechanics Reviews*, Vol. 46, No. 10, 1993, pp. 485–506. doi:10.1115/1.3120310

[11] Merlin, P. W., "Design and Development of the Blackbird: Challenges and Lessons Learned," *47th AIAA Aerospace Sciences Meeting*, AIAA 2009-1522, Jan. 2009.

[12] Wilcox, M. W., and Clemmer, L. E., "Large Deflection Analysis of Heated Plates," *Journal of the Engineering Mechanics Division*, Vol. 20, Dec. 1964, pp. 165–189.

[13] Prabhu, M. S. S., and Durvasula, S., "Thermal Post-Buckling Characteristics of Clamped Skew Plates," *Computers and Structures*, Vol. 6, No. 3, 1976, pp. 177–185. doi:10.1016/0045-7949(76)90027-4

[14] Paterson, J., "Overview of Low Observable Technology and Its Effects on Combat Aircraft Survivability," *Journal of Aircraft*, Vol. 36, No. 2, 1999, pp. 380–388. doi:10.2514/2.2468

[15] Holzapfel, G. A., *Nonlinear Solid Mechanics: A Continuum Approach for Engineering*, Wiley, West Sussex, England, U.K., 2000, pp. 55–130.

[16] *Metallic Materials and Elements for Aerospace Vehicle Structures*, U.S. Dept. of Defense, MIL-HDBK-5H, 1998.

[17] "CYCOM 5250-4 Prepreg System—Technical Data Sheet," Cytec Engineered Materials TR AECM-00008, Woodland Park, NJ, March 2012.

[18] Gonczy, S. T., and Sikonia, J. G., "Nextel 312/Silicon Oxycarbide Ceramic Composites," *Handbook of Ceramic Composites*, edited by Bansal, N. P., Springer, New York, 2005, pp. 347–373, Chap. 15.

[19] Park, I., and Grandhi, R. V., "Quantifying Multiple Types of Uncertainty in Physics-Based Simulation Using Bayesian Model Averaging," *AIAA Journal*, Vol. 49, No. 5, 2011, pp. 1038–1045. doi:10.2514/1.J050741

[20] Riley, M. E., Grandhi, R. V., and Kolonay, R., "Quantification of Modeling Uncertainty in Aeroelastic Analyses," *Journal of Aircraft*, Vol. 48, No. 3, 2011, pp. 866–873. doi:10.2514/1.C031059

[21] Quiroz, R., Embler, J., Jacobs, R., Tzong, G., and Liguore, S., "AVIATR: Predictive Capability for Hypersonic Structural Response and Life Prediction: Phase II—Detailed Design of Hypersonic Cruise Vehicle Hot-Structure," U.S. Air Force Research Lab. TR-AFRL-RQ-WP-TR-2012-0265, Wright–Patterson AFB, OH, 2012.